From linear to circular polarized light: Floquet engineering in Kitaev-Heisenberg materials with Lissajous figures

Pascal Strobel [1] and Maria Daghofer [1,2]

[1]*Institut für Funktionelle Materie und Quantentechnologien, Universität Stuttgart, 70550 Stuttgart, Germany*

[2]*Center for Integrated Quantum Science and Technology, University of Stuttgart, Pfaffenwaldring 57, 70550 Stuttgart, Germany*

(Received 10 February 2023; revised 15 May 2023; accepted 10 July 2023; published 18 July 2023)

This paper discusses Floquet engineering with arbitrary polarization in α-$RuCl_3$. We describe the influence of arbitrary polarization and the limiting cases of linear and circular polarization. The corresponding model is derived via perturbation theory up to fourth order. Starting from linear and circular polarization, we bridge the gap between those two limiting cases. We then study more complex Lissajous figures and general trends arising for them. In theory these Lissajous figures should inherit effects from both linear and circular polarized light and therefore yield tuning possibilities not yet explored in the context of candidate Kitaev materials.

DOI: 10.1103/PhysRevB.108.035132

I. INTRODUCTION

Floquet engineering has proven to be a promising tool for tuning magnetic interactions [1–3]. When light periodic in time is applied, the system can be described with a time-independent effective Hamiltonian known as a Floquet Hamiltonian [4–7]. Light frequency and amplitude then modify the system's intrinsic interactions. Therefore, modifying system properties via light is feasible. It has been shown that the procedure of an approximate time-independent Hamiltonian is, indeed, reasonable for short but experimentally accessible timescales [8] before the system experiences heating and the Floquet description breaks down. The timescale for heating has been found to increase exponentially with the driving frequency [8–10]. Timescales therefore heavily depend on the chosen driving frequency. A quantitative description of heating rates was attempted with the Floquet Fermi's golden rule [11] and linear-response theory in a rotating frame [12]. Mott insulators with strong spin-orbit coupling, which are assumed to be close to realizing a Kitaev model [13], seem to be a promising playground for Floquet engineering. In materials like α-$RuCl_3$, a Kitaev spin liquid (KSL) was proposed; however, the ground state is likely an antiferromagnet with a zigzag pattern [14]. Therefore, the idea of altering the intrinsic interaction parameters arose. There have been a plethora of attempts [15–27] to tune α-$RuCl_3$ into the KSL phase, the most promising of which to date is probably applying a magnetic field [18–23].

Most recently, there have been several proposals to tune Kitaev candidate materials into the sought after KSL via Floquet engineering. The focus here has been on either linearly polarized light [28,29], where the light angle leads to new possibilities to manipulate interactions in addition to the light frequency, or circularly polarized light, which has an isotropic influence on the system [30]. For circular polarization, an induced inverse Faraday effect [31], which is found when ligands are explicitly included via third-order perturbation theory, has been discussed. This suggests that including ligands leads to novel tuning possibilities [32,33].

Until now the transition from circularly to linearly polarized light has been lacking in the context of Kitaev-Heisenberg materials. This is particularly interesting since circularly polarized light (CPL) and linearly polarized light (LPL) each break a unique symmetry in their own right. While LPL induces interaction anisotropies, CPL breaks time reversal symmetry (TRS). Lissajous figures therefore not only connect these two special cases but also yield the possibility to study the effect of broken TRS and anisotropic interactions in combination. This could lead to unique interactions in the Kitaev-Heisenberg frame that were not available before and that may lead to novel ground-state properties. An effective model to describe arbitrary polarizations was introduced in [34–37]. Using this as a starting point, there have been proposals of tuning, e.g., Cd_3As_2 via Lissajous figures [38], with the motivation to influence magnetic symmetries via a bicircular polarized light. In this paper we want to transfer the methods of [35,36,38] to candidate Kitaev-Heisenberg models, specifically to the most promising one, α-$RuCl_3$. Our goal is to explore new tuning possibilities via Lissajous figures and to bridge the gap between linearly polarized and circularly polarized light.

To do so we derive an expression for the Peierls substitution for arbitrary polarizations. From there we obtain an effective model via perturbation theory up to fourth order to capture the formerly mentioned inverse Faraday effect, which also adds other contributions to lower-order terms. Fourth-order terms are relevant because Kitaev interactions already have fourth-order contributions in the absence of light [39]. Projecting this effective Hamiltonian onto the $j = 1/2$ basis then yields an effective Floquet-Kitaev-Heisenberg model capturing the influence of arbitrary polarized light. This model reproduces the results of the LPL [28,29] and CPL Hamiltonians [32,33] in the respective limits. We find that third- and fourth-order perturbation theory not only gives rise to the additional magnetic field for CPL but also yields additional interactions for LPL. Proceeding beyond these limiting cases, we investigate more complex Lissajous figures in order to find

different pathways for tuning Kitaev-Heisenberg materials. We try to map out the roles of the multiple variables involved in the mode, e.g., amplitude, frequency, etc.

This paper is structured as follows: In Sec. II we derive the effective model for arbitrary polarized light. We first expand the model in [29] in order to obtain the second-order terms and then calculate third- and fourth-order terms for arbitrary polarizations, similar to [32]. We give an expression for all interactions arising and briefly discuss the their nature. In Sec. III we analyze the model derived in Sec. II. The focus is first on light with a phase shift of $\epsilon = 0$ and $\epsilon = \pi/2$ in Sec. III A. Here we study a frequency multiplicity of $N = 1$ in (1), representing CPL and LPL at a driving frequency significantly above any resonances. We compare our results to the results of [32] in order to confirm the validity of our model. In Sec. III B we treat the phase shift ϵ as a free parameter. Subsequently, we continuously go from CPL to LPL and study the change in the interaction parameters. Building upon the results of Sec. III A, we start with the same driving frequency. In order to assess the influence of driving frequency we also study the case of driving between resonances of the effective Floquet Hamiltonian [29]. Last, but not least, in Sec. III C we investigate the influence of the second Lissajous parameter, the frequency multiplicity N in (1). We conclude and summarize the results in Sec. IV.

II. THEORY AND METHODS

A. Floquet Hamiltonian

As shown in [29], one can describe the kinetic part of the Hamiltonian with a Hubbard Hamiltonian in which the hopping part is modulated via the Peierls substitution $t \to t\,\mathcal{B}[\vartheta, \mathbf{A}(\tau)]$ and therefore depends on the time τ.

Since we want to consider arbitrary polarization, we describe the vector potential as

$$\mathbf{A} = \begin{pmatrix} \frac{E_x}{\omega}\sin(\omega\tau) \\ \frac{E_y}{N\omega}\sin(N\omega\tau + \epsilon) \end{pmatrix}, \tag{1}$$

where N is the ratio between the frequency in the x direction and that in the y direction $N\omega$ and ϵ describes the phase shift between x and y polarized light. This gives rise to a Peierls substitution of the form

$$\mathcal{B}(\vartheta, \mathbf{A}) = \exp\left[i\mathbf{A}\begin{pmatrix}\cos(\vartheta)\\ \sin(\vartheta)\end{pmatrix}\right], \tag{2}$$

with ϑ being the bond angle of the respective nearest-neighbor bond $\langle ij\rangle$. In the honeycomb lattice, there are three different nearest-neighbor d-d bond types, z ($\vartheta = 0$), x ($\vartheta = 2\pi/3$), and y ($\vartheta = 4\pi/3$). In addition, we have d-p bonds at an angle of $\vartheta = \pm\pi/4$ to the respective bond. The expression in (2) captures all possible Lissajous figures via the tuning parameters N and ϵ. Evidently, at $E_0 = 0$ the Peierls substitution becomes $\mathcal{B} = 1$, and the Hamiltonian describes the system in the absence of a light field. Fixing $N = 1$, ϵ gradually shifts polarization from circular ($\epsilon = \pi/2$) to linear ($\epsilon = 0$). Choosing $N > 1$ yields Lissajous figures that have not been investigated in the context of α-$RuCl_3$ so far. Unlike in [29], we focus on $\varphi = \pi/4$ as angle of LPL, i.e., $E_x = E\cos(\varphi) = E_0$ and $E_x = E\sin(\varphi) = E_0$. φ simply guarantees $E_x = E_y$ in this paper and therefore has no further influence.

The Hamiltonian for the z bonds can then be written as

$$\begin{aligned} H^z_{\mathrm{kin}}(\tau) = &-\sum_{\sigma,\langle ij\rangle_z} \mathcal{B}(0,\mathbf{A})\mathbf{d}^\dagger_{i,\sigma}\mathbf{T}^z\mathbf{d}_{j,\sigma} \\ &+ t_{pd}\left[\mathcal{B}\left(-\frac{\pi}{4},\mathbf{A}\right)(d^\dagger_{zx,i,\sigma}p_{1,\sigma} - p^\dagger_{2,\sigma}d_{yz,j,\sigma}) \right. \\ &\left. + \mathcal{B}\left(\frac{\pi}{4},\mathbf{A}\right)(d^\dagger_{zx,i,\sigma}p_{2,\sigma} - p^\dagger_{1,\sigma}d_{yz,j,\sigma}) + \mathrm{H.c.}\right], \end{aligned} \tag{3}$$

where $\mathbf{d}_{i,\sigma}$ ($\mathbf{d}^\dagger_{i,\sigma}$) denotes the vector of annihilation (creation) operators $d_{i\alpha\sigma}$ ($d^\dagger_{i\alpha\sigma}$) that annihilate (create) an electron in the d orbital $\alpha \in [xy, yz, zx]$ on site i with spin σ. The matrix $\mathbf{T}^z$ contains direct d-d hoppings [29] modified by the Peierls substitution $\mathcal{B}(0,\mathbf{A})$. $p_{i,\sigma}$ ($p^\dagger_{i,\sigma}$) annihilates (creates) a p electron on the ligand ion, and t_{pd} is the hopping between d and p orbitals. The kinetic Hamiltonian in the y and x directions can be derived by adjusting ϑ and choosing the corresponding hopping processes $\mathbf{T}^\gamma$ [29,40] as well as t_{pd}. We explicitly included the hopping processes from the d orbitals to the p ligand since it has been shown that they cannot be simply be integrated out [32,33].

The on-site interactions are captured with the Kanamori Hamiltonian

$$\begin{aligned} H_{\mathrm{int}} = &\,U\sum_{i,\alpha} n_{i\alpha\uparrow}n_{i\alpha\downarrow} + U'\sum_{i,\sigma}\sum_{\alpha<\beta} n_{i\alpha\sigma}n_{i\beta-\sigma} \\ &- J_H\sum_{i,\alpha\neq\beta}(d^\dagger_{i\alpha\uparrow}d_{i\alpha\downarrow}d^\dagger_{i\beta\downarrow}d_{i\beta\uparrow} - d^\dagger_{i\alpha\uparrow}d^\dagger_{i\alpha\downarrow}d_{i\beta\downarrow}d_{i\beta\uparrow}) \\ &+ (U' - J_H)\sum_{i,\sigma}\sum_{\alpha<\beta} n_{i\alpha\sigma}n_{i\beta\sigma} + \Delta\sum_{i,\sigma} p^\dagger_{i\sigma}p_{i\sigma}, \end{aligned} \tag{4}$$

where U is the intraorbital interaction, interorbital interaction $U' = U - 2J_H$, J_H is Hund's coupling, and $n_{i\alpha\sigma}$ is the density.

The complete Hamiltonian is periodic in time. Floquet's theorem [41] shows that such Hamiltonians can be described with a time-independent Floquet Hamiltonian [35]. In our case, the Hamiltonian takes the form

$$H^F = -\sum_{l,n} H^l_{\mathrm{kin}}\,|n+l\rangle\langle n| + \sum_l (H_{\mathrm{int}} + l\omega)\,|l\rangle\langle l|, \tag{5}$$

where l and n are the number of photons. H^l_{kin} describes a hopping process with the absorption of l photons and can be derived via averaging over time,

$$H^l_{\mathrm{kin}} = \frac{\omega}{2\pi}\int_0^{2\pi/\omega} H_{\mathrm{kin}}(\tau)e^{-il\omega\tau}d\tau. \tag{6}$$

The only time-dependent term in $H_{\mathrm{kin}}(\tau)$ (3) is the Peierls substitution $\mathcal{B}$. Performing the integration for this term yields

$$\mathcal{B}_l(\vartheta,\mathbf{A}) = \sum_n \mathcal{J}_{l-Nn}\left(\frac{E_0}{\omega}\cos(\vartheta)\right)\mathcal{J}_n\left(\frac{E_0}{N\omega}\sin(\vartheta)\right)e^{i\epsilon n}, \tag{7}$$

where we used the Jacobi-Anger expansion [7] to simplify the expression. The Floquet Hamiltonian therefore has the exact

same hopping processes as the bare Hamiltonian, but with dressed hopping strengths that now depend on ϵ, N, E_0, ϑ, and ω.

B. Second-order perturbation theory

α-$RuCl_3$ is considered to be a Mott insulator, where the Coulomb repulsion U is much larger than the hopping parameters $\mathbf{T}^\gamma$ and t_{pd} of H^F_{kin}. Therefore, we can treat the kinetic part of the Floquet Hamiltonian (5) via perturbation theory. The conventional approach is to calculate an effective second-order Hamiltonian

$$H^F_{\text{eff}} = \sum_{l,\alpha} \frac{H^{-l}_{\text{kin}} \left|\Psi^d_\alpha\right\rangle\left\langle\Psi^d_\alpha\right| H^l_{\text{kin}}}{\mathcal{E}_\alpha + l\omega}, \tag{8}$$

with l being the number of absorbed(emitted) photons, ω being the driving frequency, and $|\Psi^d_\alpha\rangle$ being the manifold of states with a double occupation on one site. Spin-orbit coupling is considered to be sizable in α-$RuCl_3$, yielding a hole in a pseudospin $j = 1/2$ state on each site like for the materials discussed in [42]. Projecting the effective Kugel-Khomskii-type Floquet Hamiltonian into the $j = 1/2$ basis then gives rise to a Kitaev-Heisenberg model like in [39].

The distinct feature of the Floquet-Kitaev-Heisenberg Hamiltonian is the dependence of the interaction parameters on ω and E_0 for CPL and, additionally, on φ for LPL [29]. In order to obtain the second-order Hamiltonian for arbitrary polarizations one has to simply exchange the Bessel functions in [29] with the expression derived in (7). The interaction parameters obtained are given in Appendix A.

In these calculations the hopping over the p-ligand atoms is integrated out and is included in the t_2 hopping $t_2 \to t_2 + t^2_{pd}/\Delta$ [29,40]. While this is valid in the case of systems without driving [39], a light field induces a complex phase for each hopping (2), which precludes including t_{pd} in the t_2 hopping. We therefore have to calculate virtual t_{pd}-hopping strengths explicitly, necessitating perturbation theory up to fourth order.

C. Third-order perturbation theory

Third-order perturbation theory considers hopping processes in which one $d \to d$ process is mediated by a ligand p atom, i.e., occurs along a d-p-d path. For CPL several theoretical studies proposed an inverse Faraday effect arising due to these additional hopping processes [32,33], which was also supported by recent experimental results [43]. Furthermore, [32] introduced analytic expressions for the Kitaev-Heisenberg Hamiltonian in third-order perturbation theory for CPL.

In this section we build on these findings and extend them to arbitrary polarization, deriving analytic expressions for third-order correction terms. The third-order contributions to the effective Floquet Hamiltonian can be calculated via

$$H^F_{\text{eff}} = \sum_{l,m}\sum_{\beta,\alpha} \frac{H^{-l-m}_{\text{kin}} \left|\Psi^d_\alpha\right\rangle\left\langle\Psi^d_\alpha\right| H^m_{\text{kin}} \left|\Psi^p_\beta\right\rangle\left\langle\Psi^p_\beta\right| H^l_{\text{kin}}}{[\mathcal{E}_\alpha + (m+l)\omega](\Delta + l\omega)}, \tag{9}$$

where $|\Psi^d_\alpha\rangle$ ($|\Psi^p_\alpha\rangle$) is the excited-state manifold with an additional electron in a d (p) orbital with excitation energies $\mathcal{E}_\alpha(\Delta)$. The possible energies for two electrons in a t_{2g} d shell are $\mathcal{E}_P = U - 3J_H$, $\mathcal{E}_D = U - J_H$, and $\mathcal{E}_S = U + 2J_H$. In contrast to second-order processes, where l photons get absorbed (emitted) in the first hopping process and emitted (absorbed) in the second hopping process, in the third-order process l photons get absorbed (emitted) in the $d \to p$ hopping, and another m photons get absorbed (emitted) in the $p \to d$ hopping, which then get collectively emitted (absorbed) in the $d \to d$ process so that no photons are present in the final state.

Using the projections of [32], our calculations for arbitrary polarization (see more details in Appendix C) give rise to three more interaction terms in addition to the J, K, and Γ terms present in systems without driving. The full third-order Hamiltonian projected onto the $j = 1/2$ basis then reads

$$\begin{aligned} H^3_{\text{eff}} = \sum_{\gamma,\langle i,j\rangle_\gamma} & J^3_\gamma \mathbf{S}_i\mathbf{S}_j + K^3_\gamma S^\gamma_i S^\gamma_j + \Gamma^3_\gamma\left(S^\alpha_i S^\beta_j + S^\beta_i S^\alpha_j\right) \\ & + D^3_\gamma \mathbf{e}_\gamma(\mathbf{S}_i \times \mathbf{S}_j) + \mu^3_\gamma\left(S^\alpha_i S^\alpha_j - S^\beta_i S^\beta_j\right) + h^3_\gamma\left(S^\gamma_i + S^\gamma_j\right), \end{aligned} \tag{10}$$

where $\gamma \in [x, y, z]$ labels the three bond directions in the honeycomb lattice according to the Kitaev interaction present on this specific bond and α and β are the remaining two spin directions, e.g., $\alpha = x$ and $\beta = y$ for the z bond ($\gamma = z$). h^3 is the magnetic field term mentioned above, which arises from broken time reversal symmetry and induces an inverse Faraday effect. D and μ break inversion symmetry (IS) and induce further anisotropies, respectively.

The terms for the z bond are then given as

$$\begin{aligned} K^3_z = \sum_{m,l} \frac{t^2_{pd}}{\Delta + m\omega}\Bigg[& \text{Re}\left(\mathfrak{B}^3_{l,m} + \mathfrak{B}^3_{m,l}\right)\frac{12}{9}\left(\frac{t_2}{\mathcal{E}_D + (l+m)\omega} - \frac{t_2}{\mathcal{E}_P + (l+m)\omega}\right) \\ & + \text{Im}\left(\mathfrak{B}^3_{l,m} - \mathfrak{B}^3_{m,l}\right)\frac{8}{27}\left(\frac{t_1 - t_3}{\mathcal{E}_D + (l+m)\omega} + \frac{2t_1 + t_3}{\mathcal{E}_S + (l+m)\omega} + \frac{6t_2}{\mathcal{E}_P + (l+m)\omega}\right)\Bigg], \end{aligned} \tag{11}$$

$$\Gamma^3 = \sum_{m,l} \frac{t^2_{pd}}{\Delta + m\omega}\text{Re}\left(\mathfrak{B}^3_{l,m} + \mathfrak{B}^3_{l,m}\right)\frac{4}{9}\left(\frac{t_1 - t_3}{\mathcal{E}_P + (l+m)\omega} - \frac{t_1 - t_3}{\mathcal{E}_D + (l+m)\omega}\right), \tag{12}$$

$$\mu^3_z = \sum_{m,l} \frac{-t^2_{pd}}{\Delta + m\omega}\text{Re}\left(\mathfrak{B}^3_{l,m} - \mathfrak{B}^3_{m,l}\right)\frac{4}{9}\left(\frac{t_2}{\mathcal{E}_P + (l+m)\omega} + \frac{t_2}{\mathcal{E}_D + (l+m)\omega}\right), \tag{13}$$

$$D_z^3 = \sum_{m,l} \frac{t_{pd}^2}{\Delta + m\omega} \mathrm{Re}\left(\mathfrak{B}_{l,m}^3 - \mathfrak{B}_{m,l}^3\right) \frac{8}{27} \left(\frac{2t_1 + t_3}{\mathcal{E}_S + (l+m)\omega} + \frac{t_1 - t_3}{\mathcal{E}_D + (l+m)\omega} + \frac{3(t_1 + t_3)}{\mathcal{E}_P + (l+m)\omega} \right), \tag{14}$$

$$h_z^3 = \sum_{m,l} \frac{-t_{pd}^2}{\Delta + m\omega} \mathrm{Im}\left(\mathfrak{B}_{l,m}^3 - \mathfrak{B}_{m,l}^3\right) \frac{2}{9} \left(\frac{t_1 - t_3}{\mathcal{E}_D + (l+m)\omega} + \frac{t_1 - t_3}{\mathcal{E}_P + (l+m)\omega} \right), \tag{15}$$

with t_1, t_2, t_3, and t_4, the entries of $\mathbf{T}^z$, defined as in [29,40]. Furthermore, we define

$$\mathfrak{B}_{l,m}^3 = \mathcal{B}_{-l-m}(0, \mathbf{A}) \mathcal{B}_{-l}^* \left(\frac{\pi}{4}, \tilde{\mathbf{A}} \right) \mathcal{B}_{-m}^* \left(-\frac{\pi}{4}, \tilde{\mathbf{A}} \right), \tag{16}$$

where $\mathcal{B}_l$ is introduced in (7) and $\tilde{\mathbf{A}} = \mathbf{A}/\sqrt{2}$. It is of note that in third-order perturbation theory there are no contributions to the Heisenberg term J, in contrast to the findings of [32].[1] Results for the x and y bonds can be deduced from (11)–(15) by selecting ϑ in (16) accordingly.

D. Fourth-order perturbation theory

While the inverse Faraday effect can be fully captured in third-order perturbation theory, the Kitaev interaction still lacks significant contributions that arise from fourth-order contributions. As is evident from the conventional Kitaev-Heisenberg model [39], $(t_{pd})^4$ terms, i.e., d-p-d-p-d processes, are the driving force for a sizable Kitaev term. It is therefore crucial to include terms in which both $d \to d$ hopping processes are mediated by ligand p atoms explicitly. This can be done in a fashion similar to that for second-order [Eq. (8)] and third-order [Eq. (9)] terms. The contributions to the interaction terms from fourth-order perturbation theory are then given by

$$J^4 = \sum_{n,l,m,k} \frac{t_{pd}^4 \, \delta_{n,-l-k-m} \left(\mathfrak{B}_{n,l}^4 - \mathfrak{B}_{l,n}^4\right)\left(\mathfrak{B}_{-m,-k}^{4*} - \mathfrak{B}_{-k,-m}^{4*}\right)}{[\Delta + (l+m+k)\omega](\Delta + m\omega)} \frac{2}{27} \left(\frac{1}{\mathcal{E}_D + (m+l)\omega} + \frac{3}{\mathcal{E}_P + (l+m)\omega} + \frac{2}{\mathcal{E}_S + (l+m)\omega} \right), \tag{17}$$

$$\begin{aligned} K^4 = \sum_{n,l,m,k} \frac{t_{pd}^4 \, \delta_{n,-l-k-m}}{[\Delta + (l+m+k)\omega](\Delta + m\omega)} \Bigg[& \frac{2}{3} \left(\frac{1}{\mathcal{E}_P + (l+m)\omega} - \frac{1}{\mathcal{E}_D + (l+m)\omega} \right) \left(\mathfrak{B}_{l,n}^4 \mathfrak{B}_{-m,-k}^{4*} + \mathfrak{B}_{n,l}^4 \mathfrak{B}_{-k,-m}^{4*} \right) \\ & - \frac{2}{27} \left(\frac{2}{\mathcal{E}_S + (l+m)\omega} + \frac{3}{\mathcal{E}_P + (l+m)\omega} + \frac{4}{\mathcal{E}_D + (l+m)\omega} \right) \left(\mathfrak{B}_{n,l}^4 - \mathfrak{B}_{l,n}^4 \right) \left(\mathfrak{B}_{-m,-k}^{4*} - \mathfrak{B}_{-k,-m}^{4*} \right) \Bigg], \end{aligned} \tag{18}$$

$$\mu^4 = \sum_{n,l,m,k} \frac{t_{pd}^4 \, \delta_{n,-l-k-m} \left(\mathfrak{B}_{n,l}^4 \mathfrak{B}_{-m,-k}^{4*} - \mathfrak{B}_{l,n}^4 \mathfrak{B}_{-k,-m}^{4*}\right)}{[\Delta + (l+m+k)\omega](\Delta + m\omega)} \frac{2}{18} \left(\frac{1}{\mathcal{E}_D + (l+m)\omega} - \frac{1}{\mathcal{E}_P + (l+m)\omega} \right), \tag{19}$$

where l, m, and k are the photons absorbed and emitted in the virtual hopping process and the fourth-order equivalent of (16) is given as

$$\mathfrak{B}_{n,l}^4 = \mathcal{B}_n \left(\frac{\pi}{4}, \tilde{\mathbf{A}} \right) \mathcal{B}_l \left(-\frac{\pi}{4}, \tilde{\mathbf{A}} \right). \tag{20}$$

As expected, for fourth order we have nonzero Kitaev interactions. In addition, there are contributions to the Heisenberg and μ interactions. The absence of h^4 terms explains the remarkably good agreement of the third-order h term in [32] with the numerical results.

Summarizing for arbitrary polarization, two types of interactions arise in addition to the formerly known J, K, Γ, and h terms which break the IS of the system (D) and induce further anisotropies (μ). Additionally, we found that Heisenberg interactions do not have third-order but fourth-order contributions. This in combination with Kitaev interactions having fourth-order contributions makes the inclusion of fourth-order terms a necessity. To showcase the influence of fourth-order terms in α-$RuCl_3$, we calculated Kitaev interactions depending on the driving amplitude E_0 in both third and fourth order. We use the same parameters as [32], i.e., *ab initio* results [44] and photoemission [45], in order to compare our results with [32]. These parameters are used for the remainder of this paper. The results are shown in Fig. 1. We notice, as already discussed, a significant difference at $E_0 = 0$, i.e., the absence of a light field, with Kitaev interactions in fourth order being significantly stronger than third-order results. For finite E_0 the qualitative behavior is comparable for third- and fourth-order calculations, with a maximum at $E_0 \approx 40\,\mathrm{eV}/(ed)$ and a strong suppression of Kitaev interactions for $E_0 > 50\,\mathrm{eV}/(ed)$. However, there is still a sizable difference in magnitude for finite E_0 between third- and fourth-order results throughout the parameter range considered. This in combination with the difference at $E_0 = 0$ is clear evidence of the importance of fourth-order terms.

[1] We believe the reason for that is that $d \to d \to p \to d$ processes appear to be neglected in [32] which lead to the vanishing of J^3 and a finite D^3.

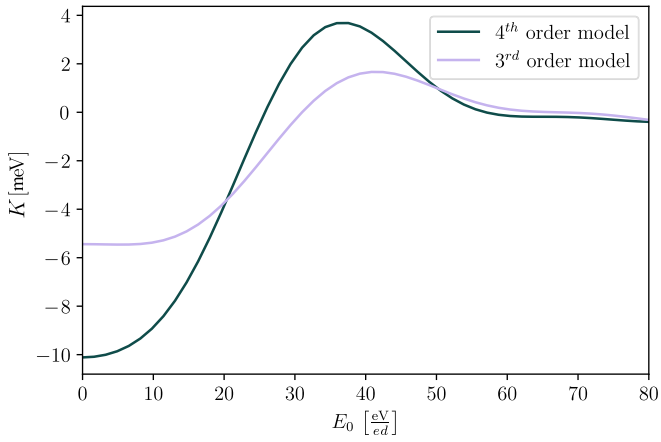

FIG. 1. Comparison of the Kitaev interaction depending on E_0 at $\omega = 12.0\,\text{eV}$ obtained with the third-order model (purple curve) and the fourth-order model (dark green curve).

III. RESULTS: FROM LINEAR TO CIRCULAR POLARIZED LIGHT

A. Limiting cases $\epsilon = 0$ and $\epsilon = \pi/2$

We start our analysis of Lissajous figures with CPL and LPL, i.e., $\epsilon = \pi/2$ and $\epsilon = 0$. The results for $\omega = 12.0\,\text{eV}$ are displayed in Figs. 2(a) and 2(b) for LPL and CPL, respectively. $E_0 = 0$ reproduces the results of the Kitaev-Heisenberg model without driving, which can be seen in (1).

Looking at Fig. 2(a), we immediately note the anisotropic influence of light on the different bond directions for all interactions as already reported in [29]. In addition, we observe no induced magnetic field h for any considered amplitudes E_0. Contrary to CPL, LPL does not break TRS and therefore does not induce a magnetic field. However, the terms D and μ make finite contributions for a nonzero amplitude E_0, and therefore, IS is broken. These terms were not reported in [29] because they arise only in third and higher orders, as discussed in Sec. II C. We therefore find that including third and higher orders explicitly is essential for arbitrary polarization.

The results for CPL are displayed in Fig. 2(b). Since CPL affects all bond directions in the same manner, the x, y, and z interactions coincide. As already reported in [33], there is a finite induced magnetic field pointing in the $\mathbf{n} = (1, 1, 1)$ direction. Meanwhile, D and μ vanish for CPL light, which was already evident from (13), (14), and (19). We report that the results from our analytical expressions (11)–(15) and (17)–(19), with fourth-order terms and third-order terms, appear to fit the ED results from [32] far better than the analytical results of [32].[2] Especially, the Kitaev term with sizable positive values around $E_0 \approx 40\,\text{eV}/(ed)$ is remarkably close to the numerical results. Even our third-order results show good qualitative agreement with the numerical results, as can be seen in Fig. 1.

For the two limiting cases of CPL and LPL we find that linear polarizations induce D and μ. In addition LPL causes a bond anisotropy depending on the light angle, which is discussed in more detail in [29]. CPL breaks TRS and therefore induces a magnetic field while keeping bond interactions isotropic.

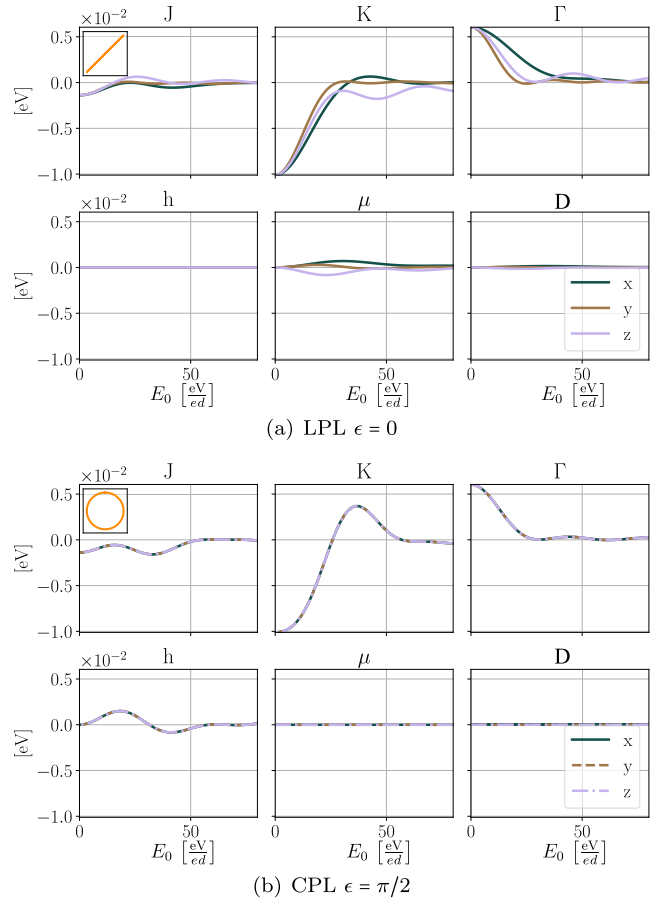

(a) LPL $\epsilon = 0$

(b) CPL $\epsilon = \pi/2$

FIG. 2. J, K, Γ, D, μ, and h interactions in the x, y, and z directions depending on light amplitude E_0 at $\omega = 12.0\,\text{eV}$. Results for frequency multiplicity $N = 1$ are shown.

B. Elliptical Lissajous figures ($N = 1$)

In this section we exploit the advantage of the Lissajous formalism (Sec. II), continuously varying ϵ between the limiting cases introduced in Sec. III A. We analyze how interactions depend on ϵ and E_0 for $N = 1$ and $\omega = 12.0\,\text{eV}$ in order to compare our results to the CPL results from [32]. The results for all interactions are displayed in Fig. 3.

As already discussed in Sec. II, interactions are bond isotropic for CPL. Moving away from CPL, the interactions become anisotropic immediately; that is, if one desires to tune all bonds in the same manner, one has to use CPL. For the J, K, and Γ interactions [Fig. 3(a)] one observes a decrease in interaction strength for $E_0 > 10\,\text{eV}/(ed)$ accompanied by the introduction of some sizable anisotropies moving from $\pi/2$ to 0. For the z-bond J and K interactions we observe a change in sign for finite E_0. Γ interactions are mainly suppressed for sizable E_0 at $\omega = 12.0\,\text{eV}$.

As already reported for CPL D and μ vanish. However, tuning $\epsilon \to 0$ induces finite values for both D and μ. We

[2]We attribute the small differences for $\omega = 12.0\,\text{eV}$ to the indices in (23) in the supplemental material of [32], which are different to the ones we calculated.

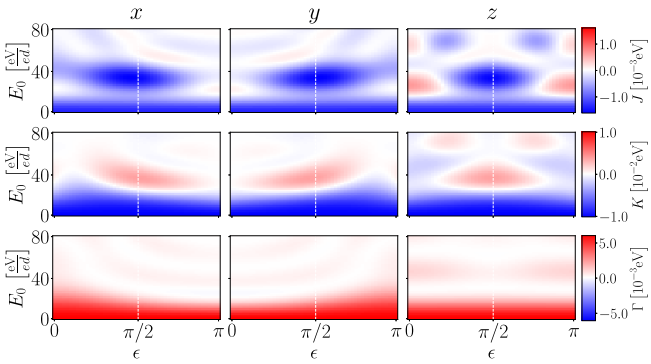

(a) J, K, and Γ interactions

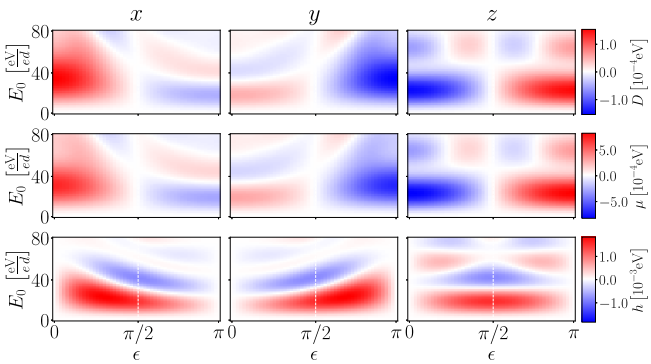

(b) D, μ, and h interactions

FIG. 3. Interactions in the x, y, and z directions depending on light amplitude E_0 and phase shift ϵ at $\omega = 12.0\,\mathrm{eV}$. Frequency multiplicity $N = 1$.

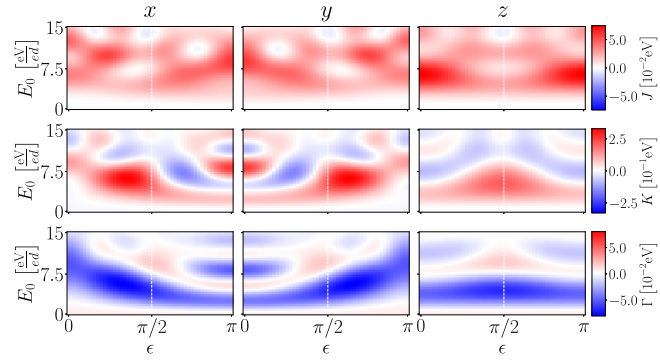

(a) J, K, and Γ interactions

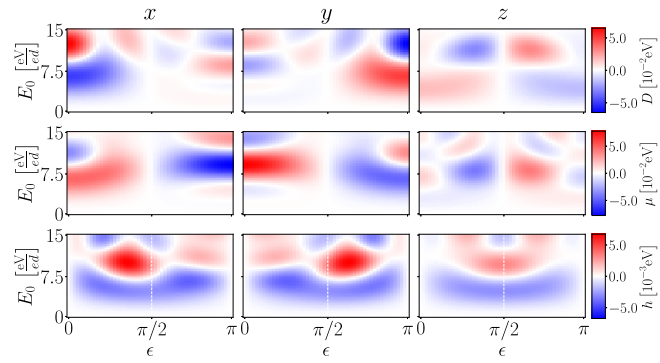

(b) D, μ, and h interactions

FIG. 4. Interactions in the x, y, and z directions depending on light amplitude E_0 and phase shift ϵ at $\omega = 2.1\,\mathrm{eV}$. Frequency multiplicity $N = 1$.

observe that D and μ are anisotropic through the entire parameter range. Contributions become strong around the limit of LPL. We note that the z terms of D and μ are antisymmetric around $\pi/2$, while other z-interaction terms are symmetric around $\pi/2$. x and y interactions for D and μ also show a unique ϵ dependence. While for the latter x interactions coincide with the y interactions when changing $\epsilon \to -\epsilon$, for D and μ there is a change in sign for the interactions. We attribute this behavior to the anisotropic nature of these interactions.

Finally, the magnetic field h, like for J, K, and Γ interactions, becomes anisotropic moving away from CPL. This can be interpreted as a change in direction of the induced magnetic field. While for CPL the direction is $\mathbf{n}$, for $\pi/4$ and $E_0 \approx 20\,eV/(ed)$ the magnetic field points mainly in the x direction. Increasing the driving amplitude up to $E_0 > 40\,\mathrm{eV}/(ed)$, the x and y contributions of the magnetic field vastly decrease, and we obtain an induced magnetic field which points mainly out of plane.

For frequencies far above all resonances ($\mathcal{E}_P$, $\mathcal{E}_D$, and $\mathcal{E}_S$) like $\omega = 12.0\,\mathrm{eV}$ we generally expect light to suppress interaction strengths with increasing E_0. On the other hand, frequencies between the resonances can induce a significant increase in interaction strength. This effect was already reported for both CPL [30,32] and LPL [28,29,33] and appears to be a promising route to obtain a KSL ground state. We therefore change the driving frequency to $\omega = 2.1\,\mathrm{eV}$, which is between the resonances of $\mathcal{E}_P$, $\mathcal{E}_S/2$, and Δ (see Appendix D) and evaluate all interactions.

It has to be mentioned that driving between resonances comes with an increased risk of heating [7,29], and frequencies have to be chosen cautiously. A poor choice of frequencies might well give misleading results since we are working in the off-resonance approximation [29] which diverges around resonances. This is especially true for fourth-order terms which go with $1/\Delta^2$; that is, frequencies close to the Δ resonance diverge even faster. Results for $\omega = 2.1\,\mathrm{eV}$ are shown in Figs. 4(a) and 4(b) for non-light-induced (NLI) interactions J, K, and Γ and light-induced (LI) interactions h, D, and μ, respectively.

The NLI interactions are significantly enhanced for finite E_0, compared to the interaction strengths without driving, throughout the whole considered parameter range of ϵ. Furthermore, we notice that the degree of enhancement strongly depends on ϵ. For the Heisenberg interaction, the largest interactions can be found for LPL. Meanwhile, for K and Γ interactions maxima can be found between LPL and CPL for $E_0 \approx 7\,\mathrm{eV}/(ed)$. Increasing Kitaev interactions beyond the maximal values of CPL and LPL indicates a clear advantage that complex Lissajous figures have. As discussed earlier, increasing Kitaev interactions compared to the other interactions is desirable, and while this is possible via tuning ϵ, it comes at the cost of lost isotropy. Hence, the model is no longer in the ideal Kitaev-Heisenberg picture of [39,42] and could point more towards a dimerization of the ground state or a gapped spin liquid [46]. The fact that this is especially possible between LPL and CPL emphasizes the importance of going beyond the limiting cases.

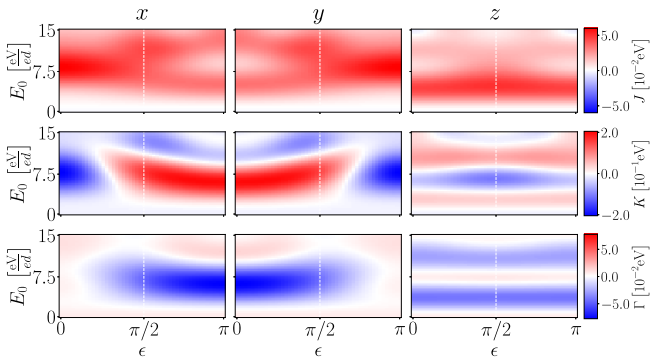

(a) J, K, and Γ interactions

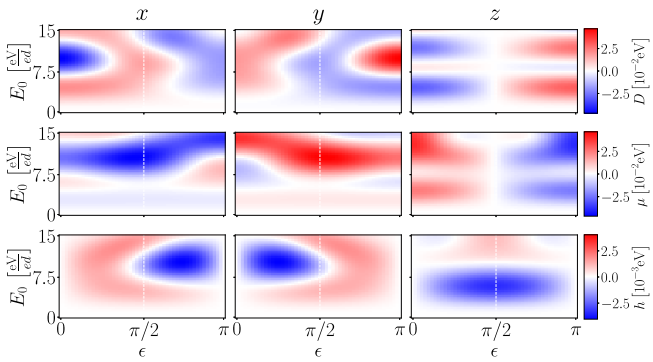

(b) D, μ, and h interactions

FIG. 5. Interactions in the x, y, and z directions depending on light amplitude E_0 and phase shift ϵ at $\omega = 2.1\,\mathrm{eV}$. Frequency multiplicity $N = 2$.

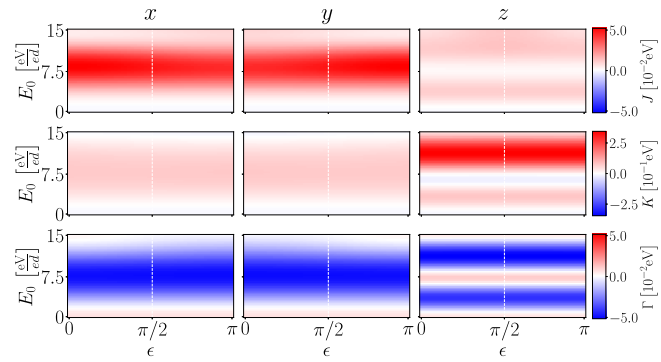

(a) J, K, and Γ interactions

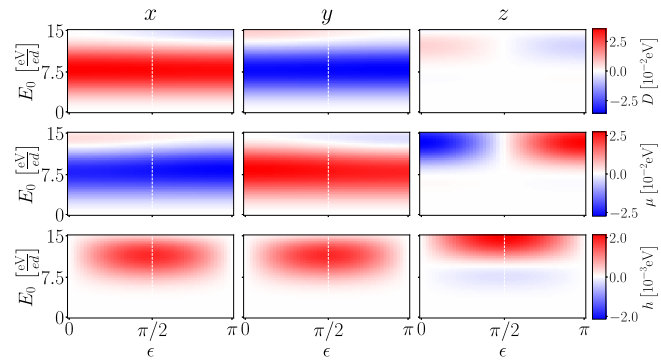

(b) D, μ, and h interactions

FIG. 6. Interactions in the x, y, and z directions depending on light amplitude E_0 and phase shift ϵ at $\omega = 2.1\,\mathrm{eV}$. Frequency multiplicity $N = 5$.

Looking at the LI interactions, we observe a significant increase in D and μ contributions. For $\omega = 12.0\,\mathrm{eV}$ both D and μ are multiple orders smaller than the NLI interactions. Meanwhile, for $\omega = 2.1\,\mathrm{eV}$, LPL, and $E_0 > 4\,\mathrm{eV}/(ed)$ their contributions increase noticeably, having the same magnitude as the NLI interactions. We observe that both D_z and μ_z are antisymmetric around $\pi/2$, which is the case for $\omega = 12.0\,\mathrm{eV}$. The induced magnetic field does not increase significantly compared to the results of $\omega = 12.0\,\mathrm{eV}$. Like for $\omega = 12.0\,\mathrm{eV}$, we note that the maximal induced magnetic field in the x and y directions is between LPL and CPL at $\epsilon \approx \pi/3$.

C. $N > 1$ Lissajous figures between resonances

After analyzing the influence of both ϵ and ω we want to discuss the influence of the frequency multiplicity N in (16) and (20). As we saw in Sec. III B and [29], driving between resonances is the most promising pathway to increase Kitaev interactions. Therefore, we set the driving frequency to $\omega = 2.1\,\mathrm{eV}$ for the remainder of this section.

We start with $N = 2$ Lissajous figures. The results for all interaction terms are displayed in Fig. 5. NLI interactions [Fig. 5(a)] show a distinct ϵ and E_0 dependency for $N = 2$. However, the magnitude of the interactions stays relatively unaffected. The most notable change is that for K and Γ the maximal interaction strength arises for LPL. Furthermore, for $\pi/2$, not all bond interactions are isotropic anymore. While x and y interactions still obey the same E_0 dependence, z interactions clearly differ from that. This is the case because $\epsilon = \pi/2$ and $N = 2$ do not correspond to CPL but to a more complex Lissajous figure, with some anisotropy (see Appendix E). The behavior of the K_x and K_y interactions yields the possibility to switch the signs of the x and y interactions by changing ϵ from 0 to π at $E_0 \approx 7.5\,\mathrm{eV}/(ed)$. For the Γ interactions this change suppresses y interactions and enhances x interactions. For both K and Γ interactions the z bond is relatively unaffected by the changes in ϵ.

In contrast to CPL, LI interactions show nonzero contributions for $\epsilon = \pi/2$ and finite E_0. Last, but not least, the induced magnetic field h has a magnitude comparable to the results in Fig. 4(b); however, the ϵ and E_0 dependence changes significantly. For $E_0 > 7.5\,\mathrm{eV}/(ed)$ in-plane contributions are more pronounced compared to the z interactions, which indicates an induced in-plane magnetic field. For smaller amplitudes $E_0 < 7.5\,\mathrm{eV}/(ed)$ we see a tendency for a magnetic field pointing out of plane.

In order to represent the behavior of the interactions for large frequency multiplicity N we set $N = 5$. The NLI interactions, displayed in Fig. 6(a), almost completely decouple from the parameter ϵ. This goes hand in hand with an almost isotropic behavior for the x and y bond interactions, with a distinct behavior for the z bond. As is evident in (2) an increase in N reduces the effect of ϵ, which is why NLI interactions are barely affected by ϵ. High N therefore offer the possibility of tuning one bond direction respective to the others, not only for $\epsilon = 0$ but also for $0 < \epsilon < \pi$. For LI interactions [Fig. 6(b)], we observe a quite distinct behavior for certain interactions.

The x and y interactions of D and μ are not ϵ dependent. Meanwhile the z interaction for both vanishes at $\epsilon = \pi/2$ and has opposite signs for $\epsilon = 0$ and $\epsilon = \pi$. One can therefore switch the signs of the z interaction while keeping the other interactions almost unchanged. Finally, the induced magnetic field vanishes for $\epsilon = 0$ and $\epsilon = \pi$ and therefore is clearly intertwined with ϵ. Significant magnetic fields just arise for relatively high amplitudes. This provides the possibility to turn the magnetic field on and off while keeping the other interactions intact. The magnetic field can therefore be controlled via the phase shift parameter ϵ.

IV. SUMMARY AND OUTLOOK

In this paper we derived an effective Floquet-Kitaev-Heisenberg Hamiltonian up to fourth-order perturbation theory, capturing the effects of driving the system with arbitrary polarization. In addition to known tuning possibilities [28,29], the relative frequency N and phase ϵ of x and y polarization become decisive factors for interaction strengths. With our model we were able to continuously go from LPL to CPL and investigate the behavior for this transition. In addition, due to the inclusion of N, we were able to capture the behavior of the interaction parameters for arbitrary Lissajous figures.

We showed that while CPL induces a magnetic field h due to TRS breaking, LPL breaks the inversion symmetry and induces the terms D and μ, which might induce interesting physical properties. Furthermore, we studied the interaction terms for different parameter settings, investigating the influence of ϵ, E_0, and N as well as ω. We showed that in order to significantly increase Kitaev interactions it is desirable to drive the system with frequencies between resonances. Moving away from CPL induces anisotropies but also increases Kitaev interactions, which might result in a gapped KSL ground state [29]. For $N > 1$ we found that $N = 2$ results in a behavior quite distinct from $N = 1$ with sizable contributions for D and μ throughout the whole parameter range of ϵ. Furthermore, we found that for higher N we have a clear tendency of J, K, and Γ to decouple from ϵ, while LI interactions still show an ϵ dependency to a certain degree. With this, tuning LI interactions, especially h, while keeping J, K, and Γ unchanged seems possible. Including third- and fourth-order terms in perturbation theory for linear polarized light is crucial because the terms D and μ appear only in third and higher orders.

Introducing arbitrary polarization into the Floquet Hamiltonian opens the doors for a multitude of yet undiscovered tuning possibilities via a plethora of parameters, making it both a very interesting and challenging topic for the future. From our studies we conclude that states like a gapped KSL with induced magnetic field could be in the range of possibilities for tuning with complex Lissajous figures. In the future it would be interesting to analyze possible ground states arising from the interactions in both isotropic and anisotropic cases.

APPENDIX A: SECOND-ORDER EFFECTIVE HAMILTONIAN FOR ARBITRARY POLARIZATION

As explained in Sec. II B, the second-order Kitaev-Heisenberg model under the influence of arbitrary polarized light can be obtained by replacing the Bessel functions in [29] with $\mathcal{B}_l(\vartheta, \mathbf{A})$ derived in Sec. II A with (7). In (6a)–(6c) of [32] we set $\mathcal{J}_l\mathcal{J}_l \to \mathcal{B}_l^*\mathcal{B}_l = |\mathcal{B}_l|^2$. $\mathcal{B}_l^*$ here describes the hopping back to the initial site with an emission of l photons. Therefore, the interactions J, K, and Γ become

$$J^2 = \sum_{l=-\infty}^{\infty} |\mathcal{B}_l(\vartheta, \mathbf{A})|^2 \frac{4}{27}\left(\frac{6t_1(t_1+2t_3)}{U-3J_H-l\omega} + \frac{2(t_1-t_3)^2}{U-J_H-l\omega} + \frac{(2t_1+t_3)^2}{U+2J_H-l\omega}\right), \tag{A1}$$

$$K^2 = \sum_{l=-\infty}^{\infty} |\mathcal{B}_l(\vartheta, \mathbf{A})|^2 \frac{4}{9}(t_1-t_3)^2 - 3t_2^2 \times \left(\frac{1}{U-3J_H-l\omega} - \frac{1}{U-J_H-l\omega}\right), \tag{A2}$$

$$\Gamma^2 = \sum_{l=-\infty}^{\infty} |\mathcal{B}_l(\vartheta, \mathbf{A})|^2 \frac{8}{9}t_2(t_1-t_3) \times \left(\frac{1}{U-3J_H-l\omega} - \frac{1}{U-J_H-l\omega}\right). \tag{A3}$$

The term $|\mathcal{B}_l(\vartheta, \mathbf{A})|^2$ can be written as

$$|\mathcal{B}_l(\vartheta, \mathbf{A})|^2 = \left[\sum_n \mathcal{J}_{l-Nn}\left(\frac{E_0}{\omega}\cos(\vartheta)\right)\mathcal{J}_n\left(\frac{E_0}{N\omega}\sin(\vartheta)\right)\cos(\epsilon n)\right]^2 + \left[\sum_n \mathcal{J}_{l-Nn}\left(\frac{E_0}{\omega}\cos(\vartheta)\right)\mathcal{J}_n\left(\frac{E_0}{N\omega}\sin(\vartheta)\right)\sin(\epsilon n)\right]^2. \tag{A4}$$

For $\epsilon = \pi/2$ and $N = 1$ Eqs. (A1)–(A3) have to coincide with (6a)–(6c) of [32]. In Fig. 7 we display the results of CPL and arbitrary polarization for $N = 1$ and $\epsilon = \pi/2$ at $\omega = 12.0\,\mathrm{eV}$. Here we used the same hopping parameters as in the main

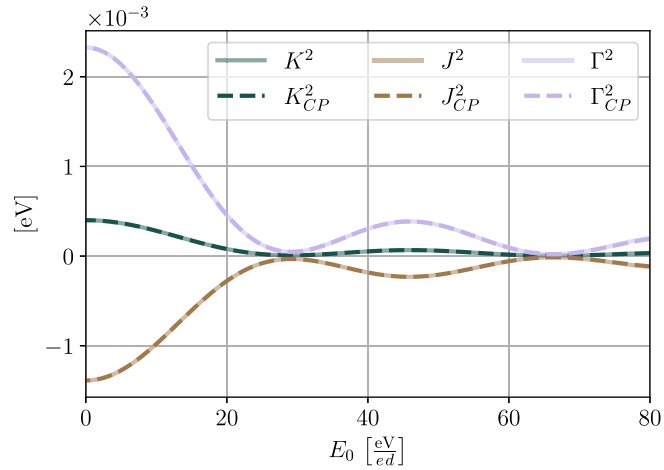

FIG. 7. Comparison of the model for CPL (dashed lines) with the second-order results for arbitrary polarization (A1)–(A3) in the limit of $N = 1$ and $\epsilon = \pi/2$ (solid lines) at $\omega = 12.0\,\mathrm{eV}$.

text. The results of the CPL model [30,32] are displayed by dashed lines, while the results of (A1)–(A3) are shown by solid lines. As expected, we observe perfect agreement between the models.

APPENDIX B: CIRCULAR POLARIZED LIGHT

Most studies to date have focused on the influence of CPL on α-$RuCl_3$ due to the induced inverse Faraday effect as well as the uniform influence of the light on all bonds. In this Appendix we will therefore study circular polarized light as a special case of third-order [Eqs. (11)–(15)] and fourth-order [Eqs. (17)–(19)] results for arbitrary polarization. In order to describe circular polarized light we have to set $N = 1$ and $\epsilon = \pi/2$ in (1). With this, expressions for third- and fourth-order terms become significantly easier to handle.

Starting with third-order terms [(11)–(15)], we obtain

$$K^3 = \sum_{m,l} \mathfrak{J}^3_{m,l}(E_0) \frac{t_{pd}^2}{\Delta + m\omega} \left\{ \frac{12}{9} \cos\left[(m-n)\frac{\pi}{4}\right] \left(\frac{t_2}{\mathcal{E}_D + (l+m)\omega} - \frac{t_2}{\mathcal{E}_P + (l+m)\omega} \right) + \sin\left[(m-n)\frac{\pi}{4}\right] \frac{8}{27} \left(6\frac{t_1}{\mathcal{E}_P + (l+m)\omega} + \frac{t_1 - t_3}{\mathcal{E}_D + (l+m)\omega} + \frac{2t_1 + t_3}{\mathcal{E}_S + (l+m)\omega} \right) \right\}, \tag{B1}$$

$$\Gamma^3 = \sum_{m,l} \mathfrak{J}^3_{m,l}(E_0) \frac{t_{pd}^2}{\Delta + m\omega} \frac{4}{9} \cos\left[(m-n)\frac{\pi}{4}\right] \left(\frac{t_1 - t_3}{\mathcal{E}_P + (l+m)\omega} - \frac{t_1 - t_3}{\mathcal{E}_D + (l+m)\omega} \right), \tag{B2}$$

$$h^3 = \sum_{m,l} \mathfrak{J}^3_{m,l}(E_0) \frac{-t_{pd}^2}{\Delta + m\omega} \frac{2}{9} \sin\left[(m-n)\frac{\pi}{4}\right] \left(\frac{t_1 - t_3}{\mathcal{E}_D - (l+m)\omega} + \frac{t_1 - t_3}{\mathcal{E}_P + (l+m)\omega} \right), \tag{B3}$$

with $\mathfrak{J}^3_{m,l}(E_0) = \mathcal{J}_{m+l}(E_0)\mathcal{J}_l(\tilde{E}_0)\mathcal{J}_m(\tilde{E}_0)$, where $\tilde{E}_0 = E_0/\sqrt{2}$. We observe that both μ and D vanish. Meanwhile, h^3, which breaks time reversal symmetry, prevails. For this reason the terms D and μ were not reported in previous studies on circular polarized light [32,33,43]. For the absence of light, i.e., $E_0 = 0$, we have only contributions for $m = l = 0$, which means that $\sin[(m-n)\pi/4] = 0$ in (B1)–(B3), while $\cos[(m-n)\pi/4] = 1$. Therefore, the magnetic field vanishes in the absence of light, and the contributions of (B1) and (B2) reproduce exactly the result for non-Floquet perturbation theory [39].

Analogous to the third-order results (B1)–(B3), fourth-order terms for CPL [(17)–(19)] yield

$$J^4 = \sum_{k,l,m} \frac{t_{pd}^4}{[\Delta + (l+m+k)\omega](\Delta + m\omega)} \mathfrak{J}^4_{m,k,l}(E_0) \frac{2}{27} \left(\frac{2}{\mathcal{E}_S + (m+k)\omega} + \frac{3}{\mathcal{E}_P + (m+k)\omega} + \frac{1}{\mathcal{E}_D + (m+k)\omega} \right) \times \left\{ \cos\left[(l-k)\frac{\pi}{2}\right] - \cos\left[(m-l)\frac{\pi}{2}\right] \right\}, \tag{B4}$$

$$K^4 = \sum_{k,l,m} \frac{t_{pd}^4}{[\Delta + (l+m+k)\omega](\Delta + m\omega)} \mathfrak{J}^4_{m,k,l}(E_0) \left\{ \frac{2}{3} \left(\frac{1}{\mathcal{E}_P + (m+k)\omega} - \frac{1}{\mathcal{E}_D + (m+k)\omega} \right) \cos\left[(m-l)\frac{\pi}{2}\right] - \frac{2}{27} \left(\frac{2}{\mathcal{E}_S + (m+k)\omega} + \frac{3}{\mathcal{E}_P + (m+k)\omega} + \frac{4}{\mathcal{E}_D + (m+k)\omega} \right) \left(\cos\left[(l-k)\frac{\pi}{2}\right] - \cos\left[(m-l)\frac{\pi}{2}\right] \right) \right\}, \tag{B5}$$

with $\mathfrak{J}^4_{m,k,l}(E_0) = \mathcal{J}_k(\tilde{E}_0)\mathcal{J}_l(\tilde{E}_0)\mathcal{J}_m(\tilde{E}_0)\mathcal{J}_{m+k+l}(\tilde{E}_0)$. Like for the third-order terms, μ vanishes for CPL, while corrections for Kitaev and Heisenberg interactions prevail. These correction terms in combination with the left-out third-order processes discussed in Sec. II C explain the discrepancies between numerical and analytical results in [32]. For $E_0 = 0$ the Heisenberg interactions vanish, while Kitaev interactions are finite, coinciding with the results of [39].

APPENDIX C: MATRIX ELEMENTS FOR INTERACTIONS

In order to project the effective spin-orbital Hamiltonian into the $j = 1/2$ basis we have to calculate the matrix elements determining all interaction parameters,

$$J = 2\,\mathrm{Re}\left(\left\langle \tfrac{1}{2}, -\tfrac{1}{2}\right| H_{\mathrm{eff}} \left|-\tfrac{1}{2}, \tfrac{1}{2}\right\rangle\right), \tag{C1}$$

$$D = 2\mathrm{Im}\left(\left\langle \tfrac{1}{2}, -\tfrac{1}{2}\right| H_{\mathrm{eff}} \left|-\tfrac{1}{2}, \tfrac{1}{2}\right\rangle\right), \tag{C2}$$

$$h = \tfrac{1}{2}\left(\left\langle \tfrac{1}{2}, \tfrac{1}{2}\right| H_{\mathrm{eff}} \left|\tfrac{1}{2}, \tfrac{1}{2}\right\rangle - \left\langle -\tfrac{1}{2}, -\tfrac{1}{2}\right| H_{\mathrm{eff}} \left|-\tfrac{1}{2}, -\tfrac{1}{2}\right\rangle\right), \tag{C3}$$

$$K = \left\langle \tfrac{1}{2}, \tfrac{1}{2}\right| H_{\mathrm{eff}} \left|\tfrac{1}{2}, \tfrac{1}{2}\right\rangle + \left\langle -\tfrac{1}{2}, -\tfrac{1}{2}\right| H_{\mathrm{eff}} \left|-\tfrac{1}{2}, -\tfrac{1}{2}\right\rangle - 2\left\langle -\tfrac{1}{2}, \tfrac{1}{2}\right| H_{\mathrm{eff}} \left|-\tfrac{1}{2}, \tfrac{1}{2}\right\rangle - J, \tag{C4}$$

$$\Gamma = -2\,\mathrm{Im}\left(\left\langle \tfrac{1}{2}, \tfrac{1}{2}\right| H_{\mathrm{eff}} \left|-\tfrac{1}{2}, -\tfrac{1}{2}\right\rangle\right), \tag{C5}$$

$$\mu = 2\,\mathrm{Re}\left(\left\langle \tfrac{1}{2}, \tfrac{1}{2}\right| H_{\mathrm{eff}} \left|-\tfrac{1}{2}, -\tfrac{1}{2}\right\rangle\right). \tag{C6}$$

The results are similar to [32], with the distinction that calculating the $\langle \frac{1}{2}, -\frac{1}{2}| H_{\mathrm{eff}} |-\frac{1}{2}, \frac{1}{2}\rangle$ and $\langle \frac{1}{2}, \frac{1}{2}| H_{\mathrm{eff}} |-\frac{1}{2}, -\frac{1}{2}\rangle$

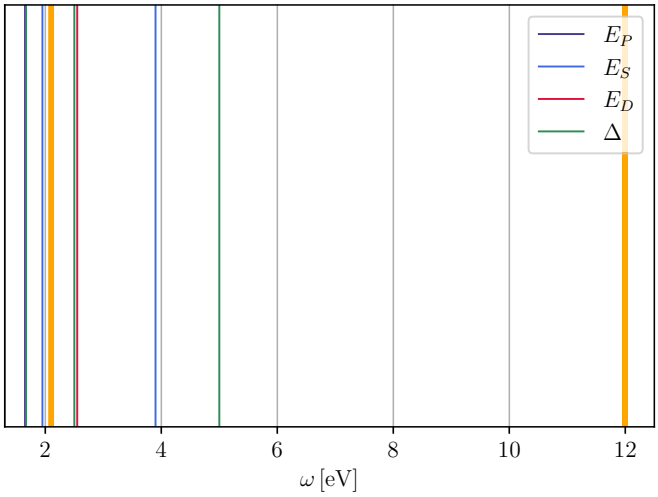

FIG. 8. Resonances of the effective Floquet-Kitaev-Heisenberg model. The resonances attributed to $\mathcal{E}_S$, $\mathcal{E}_P$, $\mathcal{E}_D$, and Δ are displayed in blue, purple, red, and green respectively. The driving frequencies used in the main text are visualized with orange lines.

elements with all hopping processes results in real and imaginary contributions. Here the element (C6) yields the Γ interactions, and (C1) yields the Heisenberg interaction, just like in [32]. The contributions (C2) and (C6) cannot be categorized as either Γ or J interactions. In order to find a physical interpretation for these contributions we mapped them back into the S_x, S_y, S_z basis, yielding

$$\tfrac{1}{2i}(S_i^- S_j^+ - S_i^+ S_j^-) = S_i^x S_j^y - S_i^y S_j^x = (\mathbf{S}_i \times \mathbf{S}_j)_z, \quad \text{(C7)}$$

$$\tfrac{1}{2}(S_i^+ S_j^+ + S_i^- S_j^-) = S_i^x S_j^x - S_i^y S_j^y, \quad \text{(C8)}$$

which are the D interactions, breaking IS, and μ interactions, inducing further anisotropies.

APPENDIX D: RESONANCE FREQUENCIES

The resonance frequencies of the system are integer multiples of the excitation energies. In addition to $\mathcal{E}_S$, $\mathcal{E}_D$, and $\mathcal{E}_P$ [29] we also have to consider Δ since we are including the p ligands explicitly in our calculation. The resonances for the considered parameter setting of $U = 3.0\,\text{eV}$ and $J_H = 0.45\,\text{eV}$ arising from the four distinct energies $\mathcal{E}_S$, $\mathcal{E}_P$, $\mathcal{E}_D$, and Δ are displayed in Fig. 8 as blue, purple, red, and green lines, respectively. The driving frequencies chosen in the main text are visualized as orange lines. The driving frequency $\omega = 12.0\,\text{eV}$ is clearly above all resonances. Meanwhile, $\omega = 2.1\,\text{eV}$ lies between the $\mathcal{E}_S/2$, $\mathcal{E}_D$, and $\Delta/2$ resonances. $\mathcal{E}_D$ and $\Delta/2$ almost coincide, which leads to more pronounced heating effects [7,29] close to this quasidouble resonance. In order to work with less pronounced heating effects, we chose a driving frequency not exactly between $\mathcal{E}_S/2$ and the double resonance but a little bit closer to the $\mathcal{E}_S/2$ resonance.

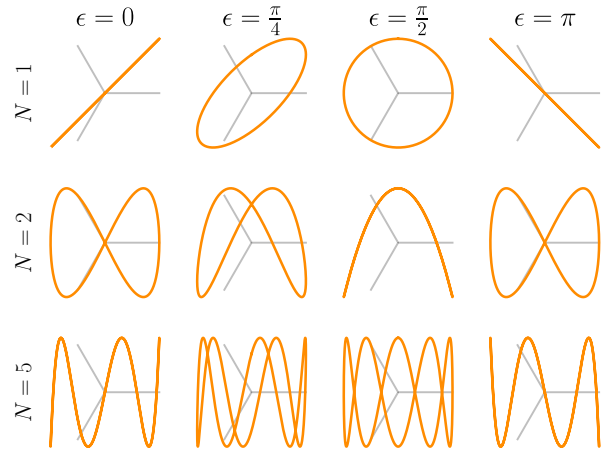

FIG. 9. Snapshots of Lissajous figures discussed in the main text. Displayed are Lissajous figures for $\epsilon = 0$, $\pi/4$, $\pi/2$, and π for $N = 1$, 2, and 5 in orange. The bond directions are shown in gray.

APPENDIX E: LISSAJOUS FIGURES

Figure 9 displays snapshots from a few Lissajous figures discussed in the main text. It becomes evident that the only Lissajous figure with a uniform influence on all bond directions (gray lines in Fig. 9) is $N = 1$ and $\epsilon = \pi/2$. The reason for the opposing behaviors of x and y interactions for $N = 1$ can be understood by looking at the Lissajous figure for $\epsilon = \pi$ and $\epsilon = 0$. $\epsilon = \pi$ is LPL rotated by $\pi/2$ compared to $\epsilon = 0$; this makes the influence of $\epsilon = 0$ on the x bond the same as $\epsilon = \pi$ on the y bond, which results in the behavior reported in the main text.

[1] A. Eckardt, *Colloquium*: Atomic quantum gases in periodically driven optical lattices, Rev. Mod. Phys. **89**, 011004 (2017).
[2] J. H. Mentink, Manipulating magnetism by ultrafast control of the exchange interaction, J. Phys.: Condens. Matter **29**, 453001 (2017).
[3] T. Oka and S. Kitamura, Floquet engineering of quantum materials, Annu. Rev. Condens. Matter Phys. **10**, 387 (2019).
[4] J. Mentink, K. Balzer, and M. Eckstein, Ultrafast and reversible control of the exchange interaction in Mott insulators, Nat. Commun. **6**, 6708 (2015).
[5] M. Bukov, M. Kolodrubetz, and A. Polkovnikov, Schrieffer-Wolff Transformation for Periodically Driven Systems: Strongly Correlated Systems with Artificial Gauge Fields, Phys. Rev. Lett. **116**, 125301 (2016).
[6] M. Claassen, H.-C. Jiang, B. Moritz, and T. P. Devereaux, Dynamical time-reversal symmetry breaking and photo-induced chiral spin liquids in frustrated Mott insulators, Nat. Commun. **8**, 1192 (2017).
[7] J. Liu, K. Hejazi, and L. Balents, Floquet Engineering of Multiorbital Mott Insulators: Applications to Orthorhombic Titanates, Phys. Rev. Lett. **121**, 107201 (2018).
[8] T. Kuwahara, T. Mori, and K. Saito, Floquet–Magnus theory and generic transient dynamics in periodically driven many-body quantum systems, Ann. Phys. (NY) **367**, 96 (2016).

[9] D. A. Abanin, W. De Roeck, and F. Huveneers, Exponentially Slow Heating in Periodically Driven Many-Body Systems, Phys. Rev. Lett. **115**, 256803 (2015).

[10] T. Mori, T. Kuwahara, and K. Saito, Rigorous Bound on Energy Absorption and Generic Relaxation in Periodically Driven Quantum Systems, Phys. Rev. Lett. **116**, 120401 (2016).

[11] T. N. Ikeda and A. Polkovnikov, Fermi's golden rule for heating in strongly driven Floquet systems, Phys. Rev. B **104**, 134308 (2021).

[12] T. Mori, Heating Rates under Fast Periodic Driving beyond Linear Response, Phys. Rev. Lett. **128**, 050604 (2022).

[13] S. M. Winter, A. A. Tsirlin, M. Daghofer, J. van den Brink, Y. Singh, P. Gegenwart, and R. Valentí, Models and materials for generalized Kitaev magnetism, J. Phys.: Condens. Matter **29**, 493002 (2017).

[14] R. D. Johnson, S. C. Williams, A. A. Haghighirad, J. Singleton, V. Zapf, P. Manuel, I. I. Mazin, Y. Li, H. O. Jeschke, R. Valentí, and R. Coldea, Monoclinic crystal structure of α-$RuCl_3$ and the zigzag antiferromagnetic ground state, Phys. Rev. B **92**, 235119 (2015).

[15] Y. Cui, J. Zheng, K. Ran, J. Wen, Z.-X. Liu, B. Liu, W. Guo, and W. Yu, High-pressure magnetization and NMR studies of α-$RuCl_3$, Phys. Rev. B **96**, 205147 (2017).

[16] Z. Wang *et al.*, Pressure-induced melting of magnetic order and emergence of a new quantum state in α-$RuCl_3$, Phys. Rev. B **97**, 245149 (2018).

[17] D. A. S. Kaib, S. Biswas, K. Riedl, S. M. Winter, and R. Valentí, Magnetoelastic coupling and effects of uniaxial strain in α-$RuCl_3$ from first principles, Phys. Rev. B **103**, L140402 (2021).

[18] I. A. Leahy, C. A. Pocs, P. E. Siegfried, D. Graf, S.-H. Do, K.-Y. Choi, B. Normand, and M. Lee, Anomalous Thermal Conductivity and Magnetic Torque Response in the Honeycomb Magnet α-$RuCl_3$, Phys. Rev. Lett. **118**, 187203 (2017).

[19] S.-H. Baek, S.-H. Do, K.-Y. Choi, Y. S. Kwon, A. U. B. Wolter, S. Nishimoto, J. van den Brink, and B. Büchner, Evidence for a Field-Induced Quantum Spin Liquid in α-$RuCl_3$, Phys. Rev. Lett. **119**, 037201 (2017).

[20] J. A. Sears, Y. Zhao, Z. Xu, J. W. Lynn, and Y.-J. Kim, Phase diagram of α-$RuCl_3$ in an in-plane magnetic field, Phys. Rev. B **95**, 180411(R) (2017).

[21] J. Zheng, K. Ran, T. Li, J. Wang, P. Wang, B. Liu, Z.-X. Liu, B. Normand, J. Wen, and W. Yu, Gapless Spin Excitations in the Field-Induced Quantum Spin Liquid Phase of α-$RuCl_3$, Phys. Rev. Lett. **119**, 227208 (2017).

[22] R. Hentrich, A. U. B. Wolter, X. Zotos, W. Brenig, D. Nowak, A. Isaeva, T. Doert, A. Banerjee, P. Lampen-Kelley, D. G. Mandrus, S. E. Nagler, J. Sears, Y.-J. Kim, B. Büchner, and C. Hess, Unusual Phonon Heat Transport in α-$RuCl_3$: Strong Spin-Phonon Scattering and Field-Induced Spin Gap, Phys. Rev. Lett. **120**, 117204 (2018).

[23] X.-G. Zhou, H. Li, Y. H. Matsuda, A. Matsuo, W. Li, N. Kurita, K. Kindo, and H. Tanaka, Intermediate quantum spin liquid phase in the Kitaev material α-$RuCl_3$ under high magnetic fields up to 100 T, arXiv:2201.04597.

[24] S. Biswas, Y. Li, S. M. Winter, J. Knolle, and R. Valentí, Electronic Properties of α-$RuCl_3$ in Proximity to Graphene, Phys. Rev. Lett. **123**, 237201 (2019).

[25] A. Koitzsch, C. Habenicht, E. Müller, M. Knupfer, B. Büchner, S. Kretschmer, M. Richter, J. van den Brink, F. Börrnert, D. Nowak, A. Isaeva, and T. Doert, Nearest-neighbor Kitaev exchange blocked by charge order in electron-doped α-$RuCl_3$, Phys. Rev. Mater. **1**, 052001(R) (2017).

[26] S.-H. Baek, H. W. Yeo, S.-H. Do, K.-Y. Choi, L. Janssen, M. Vojta, and B. Büchner, Observation of a random singlet state in a diluted Kitaev honeycomb material, Phys. Rev. B **102**, 094407 (2020).

[27] G. Bastien, M. Roslova, M. H. Haghighi, K. Mehlawat, J. Hunger, A. Isaeva, T. Doert, M. Vojta, B. Büchner, and A. U. B. Wolter, Spin-glass state and reversed magnetic anisotropy induced by Cr doping in the Kitaev magnet α-$RuCl_3$, Phys. Rev. B **99**, 214410 (2019).

[28] N. Arakawa and K. Yonemitsu, Polarization-dependent magnetic properties of periodically driven α-$RuCl_3$, Phys. Rev. B **104**, 214413 (2021).

[29] P. Strobel and M. Daghofer, Comparing the influence of Floquet dynamics in various Kitaev-Heisenberg materials, Phys. Rev. B **105**, 085144 (2022).

[30] N. Arakawa and K. Yonemitsu, Floquet engineering of Mott insulators with strong spin-orbit coupling, Phys. Rev. B **103**, L100408 (2021).

[31] S. Banerjee, U. Kumar, and S.-Z. Lin, Inverse Faraday effect in Mott insulators, Phys. Rev. B **105**, L180414 (2022).

[32] U. Kumar, S. Banerjee, and S.-Z. Lin, Floquet engineering of Kitaev quantum magnets, Commun. Phys. **5**, 157 (2022).

[33] A. Sriram and M. Claassen, Light-induced control of magnetic phases in Kitaev quantum magnets, Phys. Rev. Res. **4**, L032036 (2022).

[34] P. Mohan, R. Saxena, A. Kundu, and S. Rao, Brillouin-Wigner theory for Floquet topological phase transitions in spin-orbit-coupled materials, Phys. Rev. B **94**, 235419 (2016).

[35] V. L. Quito and R. Flint, Floquet Engineering Correlated Materials with Unpolarized Light, Phys. Rev. Lett. **126**, 177201 (2021).

[36] V. L. Quito and R. Flint, Polarization as a tuning parameter for Floquet engineering: Magnetism in the honeycomb, square, and triangular Mott insulators, Phys. Rev. B **103**, 134435 (2021).

[37] T. Nag, R.-J. Slager, T. Higuchi, and T. Oka, Dynamical synchronization transition in interacting electron systems, Phys. Rev. B **100**, 134301 (2019).

[38] T. V. Trevisan, P. V. Arribi, O. Heinonen, R.-J. Slager, and P. P. Orth, Bicircular Light Floquet Engineering of Magnetic Symmetry and Topology and Its Application to the Dirac Semimetal Cd_3As_2, Phys. Rev. Lett. **128**, 066602 (2022).

[39] J. G. Rau, E. K.-H. Lee, and H.-Y. Kee, Generic Spin Model for the Honeycomb Iridates beyond the Kitaev Limit, Phys. Rev. Lett. **112**, 077204 (2014).

[40] S. M. Winter, Y. Li, H. O. Jeschke, and R. Valenti, Challenges in design of Kitaev materials: Magnetic interactions from competing energy scales, Phys. Rev. B **93**, 214431 (2016).

[41] J. H. Shirley, Solution of the Schrödinger equation with a hamiltonian periodic in time, Phys. Rev. **138**, B979 (1965).

[42] G. Jackeli and G. Khaliullin, Mott Insulators in the Strong Spin-Orbit Coupling Limit: From Heisenberg to a Quantum Compass and Kitaev Models, Phys. Rev. Lett. **102**, 017205 (2009).

[43] T. Amano, Y. Kawakami, H. Itoh, K. Konno, Y. Hasegawa, T. Aoyama, Y. Imai, K. Ohgushi, Y. Takeuchi, Y. Wakabayashi, K. Goto, Y. Nakamura, H. Kishida, K. Yonemitsu, and S. Iwai, Light-induced magnetization driven by interorbital charge

motion in the spin-orbit assisted Mott insulator α-$RuCl_3$, Phys. Rev. Res. **4**, L032032 (2022).

[44] H.-S. Kim and H.-Y. Kee, Crystal structure and magnetism in α-$RuCl_3$: An *ab initio* study, Phys. Rev. B **93**, 155143 (2016).

[45] S. Sinn, C. H. Kim, B. H. Kim, K. D. Lee, C. J. Won, J. S. Oh, M. Han, Y. J. Chang, N. Hur, H. Sato, B.-G. Park, C. Kim, H.-D. Kim, and T. W. Noh, Electronic structure of the Kitaev material α-$RuCl_3$ probed by photoemission and inverse photoemission spectroscopies, Sci. Rep. **6**, 39544 (2016).

[46] A. Kitaev, Anyons in an exactly solved model and beyond, Ann. Phys. (NY) **321**, 2 (2006).